Int J Appl Earth Obs Geoinformation 80 (2019) 145–156

Contents lists available at ScienceDirect

Int J Appl Earth Obs Geoinformation

journal homepage: www.elsevier.com/locate/jag

Spatiotemporal patterns of lithium mining and environmental degradation in the Atacama Salt Flat, Chile

Wenjuan Liu[a], Datu B. Agusdinata[a,*], Soe W. Myint[b]

[a] School of Sustainability, Arizona State University, USA
[b] School of Geographical Sciences and Urban Planning, Arizona State University, USA

ARTICLE INFO

Keywords:
Lithium mining
Environmental health
Land-use change
Drought condition
Landsat
Spatiotemporal patterns

ABSTRACT

Emerging electric-vehicle technologies and the global transition to renewable energy have driven the production of lithium batteries significantly in the past ten years. However, potential adverse impacts accompanying this transition require closer scrutiny. The purpose of this research is to assess the environmental impact and its possible correlation with lithium mining in the Atacama Salt Flat, the world's largest lithium extraction site. Using both Landsat imagery and MODIS land products, we investigate the mining areas to (1) determine area and rate of change over time, (2) analyze spatiotemporal patterns of changes in key environmental parameters, and (3) perform regression analysis between lithium mining activities and environmental degradation between 1997 and 2017. We use five environmental parameters for our analysis: Normalized Difference Vegetation Index (NDVI), Daytime Land Surface Temperature (Day-LST), Soil Moisture Index (SMI), Nighttime Land Surface Temperature (Night-LST), and Net Evapotranspiration (ET). Our analysis shows that lithium mining operations have expanded rapidly by 7.07% annually. Our pixel-based time-series trend analysis for each image stack, using the Mann-Kendall test and Sen's slope coefficient, shows some significant degradation over the past 20 years including (1) vegetation decline, (2) elevating daytime temperatures, (3) decreasing trend of soil moisture, and (4) increasing drought condition in national reserve areas. However, no substantial degradation in nighttime-LST and ET is observed in the study area. Our analyses of the relationship between mining activities and environmental degradation also indicate that the continuous expansion of lithium mining has strong negative correlations with the NDVI and SMI, and a strong positive correlation with LST. We identified lithium mining activities as one of the major stressors to the local environmental degradation. The results provide a baseline to evaluate future socio-environmental impacts of lithium mining in the region. We anticipate our analysis will help inform mining and environmental regulators, lithium industry decision-makers, and national park managers to provide better management of the world's largest lithium production sites for a sustainable future.

1. Introduction

The world is increasingly shifting towards sustainable-energy based transportation systems, in which more sustainable forms of energy production as well as consumption are timely and strongly needed. However, potential environmental impacts alongside the transition require a closer scrutiny (Agusdinata et al., 2018). Such an energy transformation and supporting infrastructure rely on among others lithium-ion batteries as efficient high-density energy storage (Jaskula, 2017). In response to increased lithium demand for battery applications, global lithium production has risen by 12% in 2016 (IFC (International Finance Corporation), 2017) and is projected to keep growing rapidly in the near future (Deetman et al., 2018).

Most of the world's lithium production takes place in South America where 70% of global reserves are concentrated (Jaskula, 2018). Chile, as a leading producer, takes up an average of 38% of worldwide lithium production in the past twenty years (Fig. 1). The lithium mining industry in Chile started in the late 1970s and experienced dramatic and continuous expansion in production since 1997, from 4500 ton/yr to 14,100 ton/yr in 2017 (Jaskula, 2018; Joyce, 1998). The lithium extraction sites are located in the Atacama Salt Flat (ASF), Northern Chile, where the extremely arid climate and unique topography produce the saline groundwater containing 0.15% lithium that serves as the major water source for lithium extraction (Salas et al., 2010; Tran and Luong, 2015). Generally, the saline groundwater (brine) containing lithium is pumped through a cascade of ponds where impurities or by-products such as halite, sylvanite, and carnallite are precipitated by solar evaporation, wind, and chemical additives to a concentration of

* Corresponding author at: School of Sustainability, Arizona State University, Wrigley Hall, 352, 800 Cady Mall, Tempe, AZ 85287, USA.
E-mail address: bagusdin@asu.edu (D.B. Agusdinata).

https://doi.org/10.1016/j.jag.2019.04.016
Received 27 January 2019; Received in revised form 18 April 2019; Accepted 23 April 2019

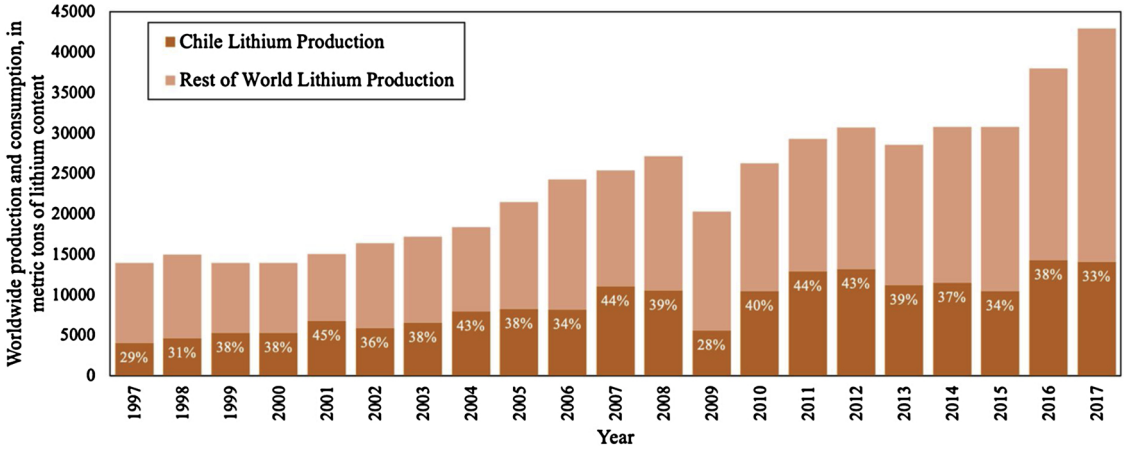

Fig. 1. Worldwide and Chile lithium production between 1997 and 2017. (Data source: USGS Mineral Commodity Summaries between 1998 and 2018 (Anon, 2019)).

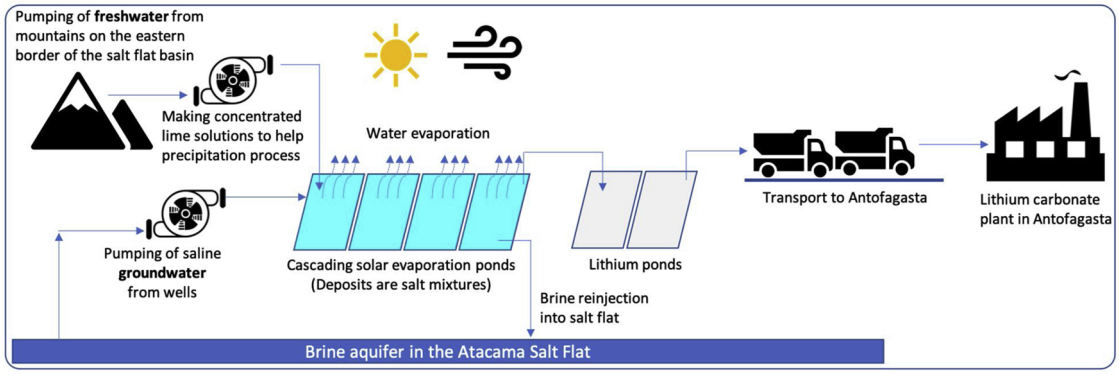

Fig. 2. Schematic representation of lithium extraction process in the ASF. Current extraction technology concentrates the brine through chemical additives and evaporation by wind and solar energy. Lithium-concentrated salt then transported to Antofagasta for further purification and production of lithium carbonate.

approximately 6000 ppm (Tran and Luong, 2015; Flexer et al., 2018). After that, the concentrated brine is transported back to the recovery plant in Antofagasta for future purification and processing. A general schematic representation for the lithium extraction process in the ASF is shown in Fig. 2.

Water usage and the potential threats to local flora and fauna are two major sustainability concerns driven by lithium extraction (Flexer et al., 2018). In the lithium extraction process, 95% of extracted brine water is evaporated (Habashi, 1997) and freshwater is pumped directly from mountains on the eastern border of the ASF. Even though the brine water is not suitable for human or agricultural consumption, it is in hydrodynamic relation with the surroundings (Marazuela et al., 2019a). As a result, the water-intensive mining process in this very arid region can cause adverse effects on aquifer depletion (Babidge and Bolados, 2018), hydric balance and ecosystems (Flexer et al., 2018; Babidge and Bolados, 2018), which raise concerns by local populations, environmentalists, and governmental authority. In the recent decade, a large number of mining permits had been issued by the regional authority to meet the globally increasing demand for lithium carbonate, such that the expanded production scale may cause changes in landscape and microclimate of the surrounding environment, resulting in social conflicts between mining firms and local communities (Molina Camacho, 2016).

This study aims at examining spatiotemporal changes in the environment of the Atacama Salt Flat (ASF) and the surrounding areas by answering the following two research questions: (1) *Which parts in the studied area have been experienced environmental degradation in the past 20 years (1997–2017), in terms of mining land use, vegetation cover, and micro-climate?* and (2) *What is the relationship between the expanding lithium industry and dynamic patterns of environmental degradation in this area?* Considering challenges in quantifying the spatiotemporal dynamics of the lithium mining production and environmental impacts in this area, we propose remote sensing approach to analyze these dynamics, providing credible baseline information of the environmental conditions for local communities, state decision-makers, park management officials and lithium mining industrial managers.

The issue of environmental degradation related to lithium mining has not been largely addressed by existing literature due to the remoteness of the site and the shortage of reliable data. The qualitative research has been conducted in this area to document the intense conflicts between communities and mining companies over water and land. Babidge (2016) studied the contested value of resources in this area through interviews with community leaders, mining workers, and indigenous people. The study analyzes how the commodification of natural resources caused by the lithium mining industry is changing water availability and other environmental factors, which in turn affecting the livelihood of the traditional agro-pastoral economy of communities. Babidge (2013) also investigated the contested moral values embedded in the “partnership” between mining companies and indigenous communities in neighboring communities through interviews, observations, and meetings. The study documented the negative changes brought by the lithium mining in the ASF, such as limited access to old pastoral territory, pollution, and rapid change to traditional culture and social practice. However, these changes as well as the relationship between environmental changes and lithium production have not been adequately quantified.

Furthermore, environmental justice issue has been attracting attention on the disputes over limited resources in the Atacama Desert.

Romero et al. (2012) explored the mining development and the environmental injustice in the Atacama Desert by assessing the water balance in selected watersheds where mining operations are mostly concentrated. GIS mapping was applied to explore the spatial relationship of mining sites, conservation areas, indigenous lands, and economic investments. However, the paper covered all mining types in Northern Chile including copper, gold, and other minerals, therefore may not reflect the unique characteristics of lithium mining. Moreover, the discussion of these spatial relationships didn't quantify the possible causal relationship between mining development and environmental parameters.

Existing literature centering on the quantification of environmental impacts of lithium mining in South America is limited in terms of the number of publications as well as the research methodology (Agusdinata et al., 2018). Life cycle assessment is the most common methodology applied in quantifying the overall environmental impacts caused by lithium carbonate production. Stamp et al. (2012) assessed the life-cycle environmental impacts lithium carbonate production in the Atacama Desert by examining Cumulative Energy Demand (CED), Global Warming Potential (GWP), and EI99, which is an average weighting indicator combing different impact categories. However, the study focused greatly on energy consumption and carbon emissions of lithium mining and did not capture the spatiotemporal patterns of impact on local water cycle and landscape, which are of great importance considering the extreme local climate.

Current literature showcased that remote sensing approach had been broadly applied to exploring landscape dynamics and ecosystem service functions. Ishtiaque et al. (2016) examined the ecosystem dynamics of the mangrove forest through MODerate Resolution Imaging Spectroradiometer (MODIS) product by comparing five ecological parameters including Percentage Tree Cover (PTC), Enhanced Vegetation Index (EVI), Net Primary Productivity (NPP), Leaf Area Index (LAI), and Evapotranspiration (ET). A pixel-based ordinary least square (OLS) regression model was then developed for time-series trend analysis of detecting the spatiotemporal changes of ecosystem health. Estoque et al. (2018) assessed the environmental impacts in Myanmar's mangrove forests caused by deforestation through Land Surface Temperature (LST), ET, terrestrial NPP, and PTC using MODIS land products. The study also quantified temporal changes in the area of mangrove deforestation through Landsat imagery. Wang et al. (2016) studied the spatiotemporal pattern of the surface urban heat island intensity in the Phoenix metropolitan area and the relationship with land use land cover (LULC) using MODIS LST images and classified LULC maps generated from Landsat imagery. A time-series trend analysis was also performed using the OLS regression model to examine the statistical significance of temperature change on a pixel basis.

To examine spatiotemporal changes in the environment of the ASF and surrounding areas, we will first introduce the unique topography, landscape attributes, and biodiversity importance of our study area. We then present the time-series trend analysis and findings. The last section discusses possible correlations between the expanding lithium industry and patterns of environmental degradation, and point out to other possible environmental stressors affecting the environmental changes in the study area.

2. Study area

The Atacama Salt Flat (ASF) (Fig. 3), located in the Region of Antofagasta, Northern Chile, is the third largest salt flat in the world (around 3000 km^2), providing crucial ecosystem services to local communities and diverse flora and fauna species. Geographically, the salt flat is an *intramontane endorheic* basin (i.e. an alluvium-filled valley within mountainous ranges with a closed drainage system) bounded by high mountains to each side (Fig. 3a). Unlike other salt flats, the topography is of a high level of roughness and seldom covered by shallow water due to the rapid evaporation process (Kampf et al., 2005). Four sectors of the Los Flamencos National Reserve (Fig. 3)- Soncor (S.4), Laguna de Aguas de Quelana (S.5), Valle de La Luna (S.6), Tambillo (S.7) - located in our studied area were created in 1990 and is governed by the Chile National Forest Corporation (CONAF). The S.4 and S.5 area are formed by permanent lagoons which support diverse biodiversity and serve as an important nesting center for flamingos. The S.6 and S.7 areas are mostly covered by barren soil and salt crests but they still provide habitats to diverse species.

Rainfall in the ASF is limited and mostly concentrated in the summertime between January and March, with annual precipitation of 10 mm in the salt flat and 140 mm on high mountains (Salas et al., 2010). Known as a high altitude region, elevation of this study area decreases gradually from surrounding mountainous sectors towards the center of the salt flat, from averagely 3300 to 2300 m above sea level (Fig. 3a). The local climate is arid and mild, with the highest daytime temperature of 24.3 °C in summer from December to February and the average lowest temperature of 0.3 °C in winter from June to August.

The area included in this study covers the ASF and its surrounding rural settlements in the north and east border of the ASF (Fig. 3a), covering a total area of 8284 km^2. Land cover land use types in the study area are mostly barren soil, rural settlements clustered in north and east margin, and mining ponds in the center of ASF. Sparsely clustered vegetation oases can be found along the streams and lagoons and near human settlements. Mining ponds can be clearly distinguished from surroundings in the center of ASF by its bright cyan color. San Pedro de Atacama located 55 km north of ASF is the largest town in this commune (the third-level administrative division of Chile), and other communities are sparsely distributed along the northeastern margin.

3. Materials and methods

3.1. Materials

This study used yearly Landsat imagery with time-series spanning from 1997 to 2017. Specifically, two images of the best quality for each year were selected, one from January to February and one from June to July. We selected images acquired at approximately the same time in both summertime and wintertime of the year to minimize the seasonality variation and the spectral variation brought by phenological effects. The images with the striping noise in 2008 winter, 2011 winter, 2012 and 2013 summer were excluded. A total of 37 Landsat imagery at a spatial resolution of 30 m were used to derive Normalized Difference Vegetation Index (NDVI), Daytime Land Surface Temperature (Day-LST), Soil Moisture Index (SMI), and mining areas. Details about acquisition date and cloud cover can be found in the Supplementary Information (SI-Table 1).

We also used MODerate Resolution Imaging Spectroradiometer (MODIS) level-2 data product for environmental indicators that cannot be directly derived from Landsat imagery. Specifically, this study used the nighttime temperature layer of MODIS 8-Day LST product (MOD11A2) from 2000 to 2017 and selected images with the same acquisition date with the Landsat imagery. MODIS yearly ET product (MOD16A3) from 2000 to 2014 was also used to map the dynamics of water loss due to soil evaporation and plant transpiration (Mu et al., 2007). Hence, a total of 36 images of Night-LST and 15 images of Net ET both at a spatial resolution of 1 km were collected for this study.

3.2. Image processing

We examined most commonly used environmental indicators, NDVI, LST in daytime and nighttime, SMI, and ET, and the area of mining production to detect statistically significant trends of environmental degradation. We followed the process of the pixel-based trend analysis method widely applied in remote sensing studies (Ishtiaque et al., 2016; Estoque et al., 2018; Wang et al., 2016; Fan et al., 2017). The detailed workflow of image processing and analysis is shown in Fig. 4.

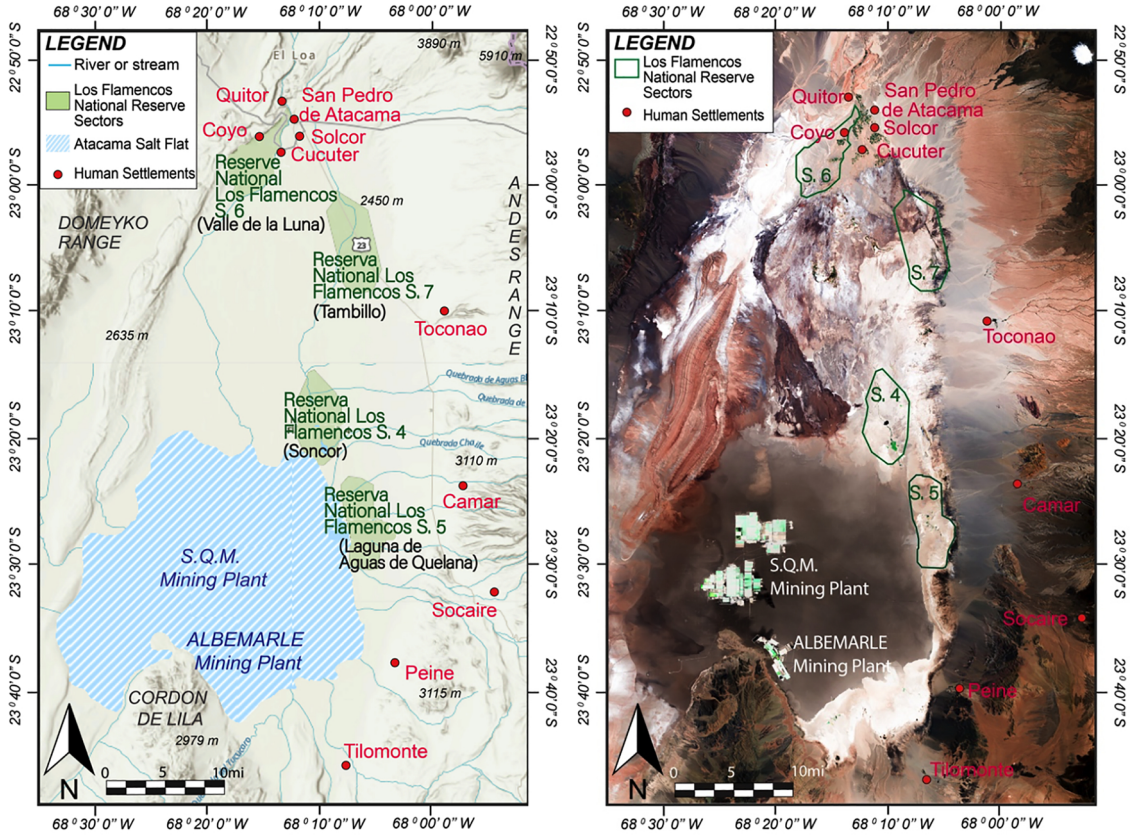

Fig. 3. Map of the study area in the ASF. The study area includes rural settlements surrounding ASF in the North and East border (red-dotted), mining companies in the center of ASF (cyan color), and four sectors of the Los Flamencos National Reserve (S.4, S.5, S.6 and S.7) bounded in the green box.

We used NDVI as an indicator for mapping green biomass, considering its extensive uses in land cover identification (DeFries and Townshend, 1994; Hansen et al., 2000), phenological studies (Lee et al., 2002; Reed et al., 1994; Studer et al., 2007), and assessing ecological responses to environmental change (Pettorelli et al., 2005). For our study, the NDVI (Running, 1990; Myneni et al., 1995) is calculated for each Landsat image as:

$$NDVI = \frac{NIR - RED}{NIR + RED} \quad (1)$$

where NIR and RED refer to the amounts of near-infrared and red light, respectively, reflected by the vegetation and captured by the satellite. In total, 35 NDVI images were generated for the study period from 1997–2017, with the valid pixel value ranging from -1 to 1.

Satellite-based data provided the only possibility of measuring LST over wide areas with high temporal resolution (Li et al., 2013), providing more accurate assessments on urban heat island effect (Ngie et al., 2014) and climate change studies in diverse spatial scales (Yang et al., 2013). In this study, we use LST to map the spatiotemporal changes of micro-climate and heating effects in the studied area. The

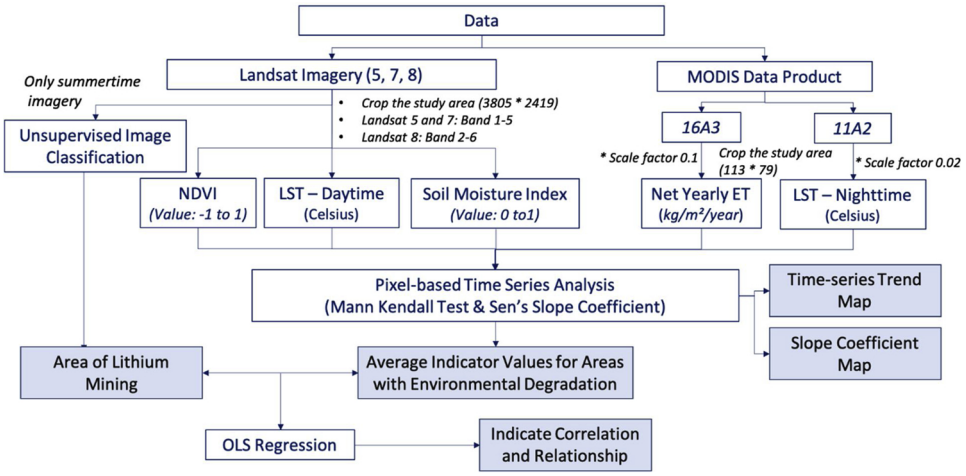

Fig. 4. Research diagram depicting the workflow of image processing and analysis.

LST is retrieved from Landsat imagery according to the method validated by (Avdan and Jovanovska (2016)), as (Artis and Carnahan, 1982):

$$T_S = \frac{BT}{\{1 + [(\frac{\lambda BT}{\rho})\ln\varepsilon_\lambda]\}} \quad (2)$$

where Ts is the LST in Celsius, BT is at-sensor brightness temperature in Celsius, λ is the wavelength of emitted radiance, ε_λ is the land surface emissivity, and ρ is calculated by Boltzmann constant, Planck's constant and velocity of light. A total of 35 LST images was derived for the study period from 1997 to 2017 with a spatial resolution of 30 m.

Soil moisture is another key aspect examined in this study for monitoring the drought conditions in the area. We use the method developed and validated by Zhan et al. (2007) to retrieve Soil Moisture Index (SMI) from Landsat imagery, which is calculated as:

$$SMI = 1 - \frac{1}{\sqrt{M^2 + 1}}(R_{NIR} + MR_{RED}) \quad (3)$$

where R_{NIR} and R_{RED} refer to the atmospherically corrected reflectance of NIR band and red band respectively, and M is the slope of soil line which is extracted using the NIR and red band reflectance of the study area (Zhan et al., 2007). In total, 35 SMI images were processed with a valid range from 0 to 1 between 1997 and 2017 at a spatial resolution of 30 m. Meanwhile, image layers of MODIS nighttime LST and Net ET were processed by multiplying with their scale factors and converted to Celsius and kg/m^2/year, respectively.

3.3. Image classification for mining and non-mining

Since little knowledge of extraction capacity in the study area is known to the public, remote sensing data provide a perfect opportunity of monitoring the expansion scale of lithium extraction. Hence, we decide to classify the imagery for mining and non-mining area for the period of 1997–2017. We only use the summertime Landsat imagery for classification since lithium production is most distinguishable from the background soil during summer months.

We performed an unsupervised classification for mining areas using the Iterative Self-Organizing Data Analysis (ISODATA) algorithm. We created 100 clusters using a maximum iteration of 10 and a convergence threshold of 0.95. Clusters were identified as either mining or non-mining through visual interpretation of the Landsat image displayed in different band combinations and with reference to Google Earth imagery. Misclassification is inevitable in every single image classification. Thus we also employed Google Earth imagery to assist in identify misclassified areas and then manually corrected misclassified areas using "Area Fill" tool in the ERDAS Imagine software.

To appropriately evaluate the classification appropriately, we conducted an accuracy assessment for each classified image. For each classified image, we created 200 stratified random validation points with minimum points of 100 for each class. The producer's accuracy, user's accuracy, overall accuracy, and Kappa coefficient for 20 classified images were calculated from the error matrix and reported in Supplementary Information (SI-Table 2). Since the cyan mining operation area within the ASF can be easily distinguished from the background barren soil, we achieved the overall accuracy exceeding 97% and the overall Kappa coefficient exceeding 0.95.

The resulted area of mining is used to calculate the area of expansion for each year as the difference in the area of mining between two consecutive years, and average expansion rate (Seto et al., 2011) as $100 \times ((\frac{MA_{2017}}{MA_{1997}})^{\frac{1}{d}} - 1)$, where MA1997 and MA2017 are the area of mining in 1997 and 2017 respectively, and d is the time span of the study in years.

3.4. Time-series trend analysis

The image processing procedure generated five stacks of Landsat and MODIS images for 1997–2017 and 2000–2017, respectively. That is, NDVI, LST, and SMI from Landsat imagery; Nighttime LST and ET from MODIS imagery. With these processed image stacks, we performed a trend analysis on each pixel stack of these indicators to explore whether an increasing or decreasing trend can be detected. The non-parametric statistical test of Mann-Kendall (MK) test (Mann, 1945; Kendall, 1948) is selected to achieve this purpose because it can perform robustly concerning the relatively small sample size, potential non-normality issue, and nonlinear relationship with the year sequence. More specifically, the time-series pixel values of each corresponding pixel stack from each Landsat and MODIS product are extracted and applied in the MK test. Pixel stacks with a calculated p-value ≤ 0.10 showing a detectable monotonic trend are retained for generating the time-series trend map. We also apply Sen's slope estimator (Sen, 1968) to calculate the slope coefficient for pixel stacks showing a detectable monotonic trend over time. Subsequently, the slope coefficient map showing the rate of change is generated for each image stack for the study period.

3.5. Correlation analysis

The other primary objective of this study is to explore possible impacts of lithium mining expansions on the local environment. Regression analysis has been widely used by remote sensing studies for establishing relationships between various remotely sensed biophysical variables (Wang et al., 2017; Chen et al., 2006; Carter, 1998; Schiebe et al., 1992). To achieve this, we applied the ordinary least square (OLS) regression method (Steel and Torrie, 1980) to measure the effect of the mining expansion on each environmental variable. In the regression model, the yearly value of areas for the mining operation is explanatory variable, and the corresponding response variable is the yearly mean value of each environmental variable for areas with a detectable degradation trend. Regression models with a calculated p-value ≤ 0.05 and an $R2 > 0.5$ are considered as indicating a strong correlation.

In order to separate the effect of climate variability and mining on the negative changes in NDVI, we excluded pixels having relatively strong correlations between NDVI and SMI in the regression analysis, considering SMI as an indicator of the impact of climate. Only pixels with weak or no correlation between NDVI and SMI (absolute value of Pearson's correlation coefficient < 0.4 (Nishishiba et al., 2014)) are retained for the regression analysis.

4. Results and analysis

4.1. Time-series changes of mining

The changes in the mining area in the ASF were determined through image classification process using the Landsat imagery. From 1997–2017, lithium mining operations were estimated to expand from 20.54 km2 to 80.53 km2 (Fig. 5). Over the past twenty years, with an average expansion rate of 7.07% per year, the mining industry in the ASF has accumulatively expanded about 60 km2, four-fold of the production scale in 1997. Spatially, mining operations started from the original ponds developed in 1997 and gradually expanded through the years (Fig. 6). A series of small separated ponds in central-left and southwest corner might be experimental ponds for future expansion purpose.

Our analysis also shows an overall trend of continuous increase in the lithium mining area and a fluctuant pattern of the yearly expanded area (Fig. 5). However, certain years showed relatively larger area in expansion, such as 1999, 2009, and 2010, indicating two major expanding activities in the past twenty years, one for SQM, a mining

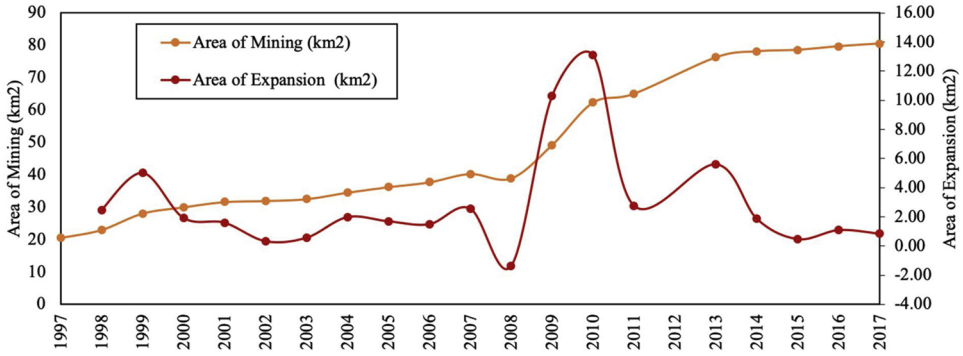

Fig. 5. Lithium mining area and area of yearly expansion in the ASF between 1997 and 2017. The lithium mining industry has accumulatively expanded about 59.99 km^2 in the past 20 years and reached four-fold of its production scale in 1997. Detailed results are available in Supplementary Information (SI-Table 3).

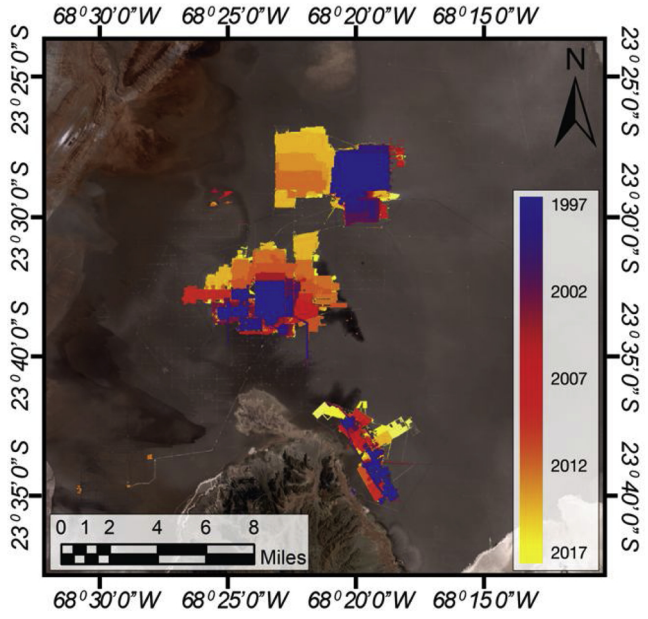

Fig. 6. Spatial map of lithium mining area in the ASF between 1997 and 2017. The color transitioning from deep blue to bright yellow represents newly developed mining area in each year.

company, entering the lithium market and the other for recovering from the economic crisis.

4.2. Time-series changes of environmental degradation

4.2.1. Vegetation cover

NDVI detects the response of vegetation varieties to the local environmental disturbance with a valid range from -1 to 1. The positive value from 0 towards 1 corresponds to vegetation cover from sparse shrub or grassland to dense canopy, and value towards -1 indicates the absence of vegetation and the presence of water bodies. Hence, a negative change of NDVI in this study can imply the degradation from dense tree cover to shrubland, from shrub or grassland to barren soil, or from barren soil to mining operation ponds.

The negative changes of NDVI are evident within the ASF (Fig. 7a), with NDVI values declined averagely from 0.0102 to -0.4077, representing a land cover change from barren soil to mining ponds over the past 20 years. The decreasing trend of NDVI is also noticeable in the northern human-settled areas where villages are distributed in clusters (Figs. 7a, 10 a). In these areas, the NDVI values declined from at least 0.025 to a maximum of 0.7331 to an average value of 0.1612 over an area of 3.4281 km^2 during the past 20 years, indicating a degradation trend towards shrubs or grasslands and an overall trend of sparser vegetated areas.

As for the national reserve sectors, the decreasing trend of NDVI is also detectable (Fig. 7a). NDVI values of sector S.6 and S.7 declined from a maximum of 0.2925 and 0.3095 to approximately 0.0850 and -0.0337, respectively, indicating the degradation of vegetated lands. In sector S.4 and S.5, NDVI values declined approximately from a wide range of −0.2617– 0.2047 to an average value of -0.0853. Such changes, however, it cannot be solely classified as vegetation degradation since these sectors are mainly composed of lagoons.

The negative changes of NDVI in the majority of areas in our study site are not detectable. However, a decrease of NDVI values is still detectable in areas of isolated rural settlements or important ecosystem functions such as along streams and near wetlands. Our analysis shows the annual negative changes in NDVI values (Fig. 7b). Mining areas had an average annual decrease of 0.0086 in NDVI values, which is faster than the average annual decrease of 0.0037 in NDVI values for human settlements in the North.

4.2.2. Land surface temperature

Our study shows that areas surrounding the mining sites within the ASF are experiencing the most severe level of increase in daytime-LST (Fig. 8a), while the increase rate is slower than other areas (Fig. 8b). Over the past 20 years, daytime-LST in areas within the ASF increased from approximately 28.4 °C in summer and 8.32 °C in winter to 32.9 °C and 14.11 °C with an average rate of 0.74% and 2.68% per year, respectively. The increasing trend of daytime-LST is also evident in the northern human-settled areas, where a total of 5.09 km^2 area is experiencing a warmer local climate during the daytime at a rate ranging from 0.127 °C to 0.455 °C per year (Fig. 10b). The national reserve sector S.5 and S.7 are more impacted by the increasing daytime-LST, compared with other reserve sectors. Specifically, about 12.42 km^2 in sector S.5 and 10.19 km^2 in sector S.7 have experienced an increasing trend of daytime-LST with an average rate of 0.231 °C and 0.259 °C per year, respectively. Margins of the ASF have also shown an increasing trend of daytime-LST in clusters, while other LST increased areas are distributed in a scattered pattern.

By contrast, in terms of nighttime-LST, neither increasing nor decreasing trend was detected in our study site. Since the study site is located in an arid desert region, the rapid cooling process of desert soil quickly brings land surface temperature back to the equilibria with air temperature during nighttime.

4.2.3. Soil moisture and evapotranspiration

Our study finds that a total 2214.5 km^2 areas in the study site are experiencing a significantly decreasing trend of soil moisture over the past 20 years. In these areas, the SMI declined from at least 0.004 index unit to a maximum of 0.96 to a range of 0.00002–0.9, with a maximum decrease rate of 0.0368 in SMI values per year. It is noticeable that the increasing drought condition is prevalent in our study area without a

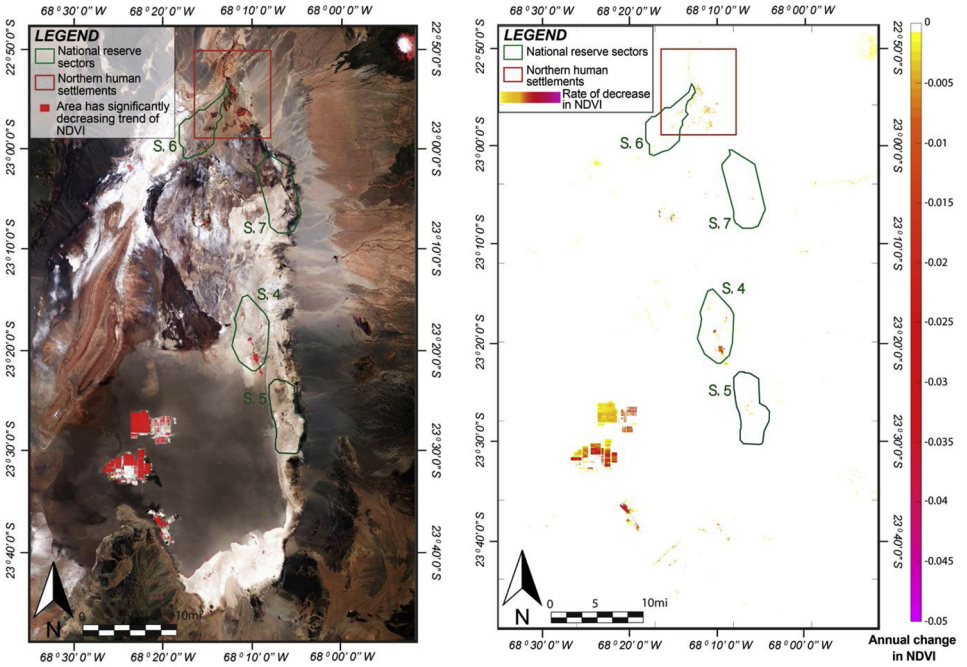

Fig. 7. (a) Map of areas experiencing a significantly decreasing trend of Normalized Difference Vegetation Index (NDVI) and (b) Map of annual decrease rate in NDVI for NDVI significantly decreased area between 1997 and 2017. The negative changes of NDVI are evident within the ASF, northern human-settled area, and some national reserve sectors. Mining areas within the ASF are encountering a faster annual decrease in NDVI comparing to other areas.

clear pattern of spatial distribution (Fig. 9a). The edges of mining ponds and southeastern margins of the ASF do have a faster rate of decline compared to the surrounding areas (Fig. 9b). Human settlements in the north side also have an increasing drought condition with an annual decline rate in SMI of 0.0018, however, the spatial pattern is still not clear for these areas (Fig. 10c).

The annual mean net ET for our study site is 48.97 kg/m^2/year in the past 20 years, while almost all the areas don't have a detectable trend of change. Only two pixels in the northeast of the ASF have experienced a loss of ET at a rate of 0.89 kg/m^2 per year.

4.3. Relationship of mining activities and environmental degradation

Since our analysis only detected changes in NDVI, daytime LST and SMI for the study area, we examined the effect of lithium mining on these changes. We excluded pixels with negative NDVI values to detect the effect of mining on degrading vegetation. We also excluded the climatic variabilities in the negative changes in NDVI by only retaining pixels with weak or no correlation between NDVI and climate. Our results show the expansion of lithium operations has strong negative correlations with NDVI and SMI and strong positive correlation with LST (Fig. 11).

The mining area is found to have a strong negative correlation with the mean values of NDVI for vegetations having detectable negative changes of NDVI (p-value = 0.000, R2 = 0.9027). The slope of regression function indicates that expanding 1 km2 of mining area could decrease the average NDVI value in degrading vegetations by 0.0014 (Fig. 11a). The relationship between the mining area and the mean

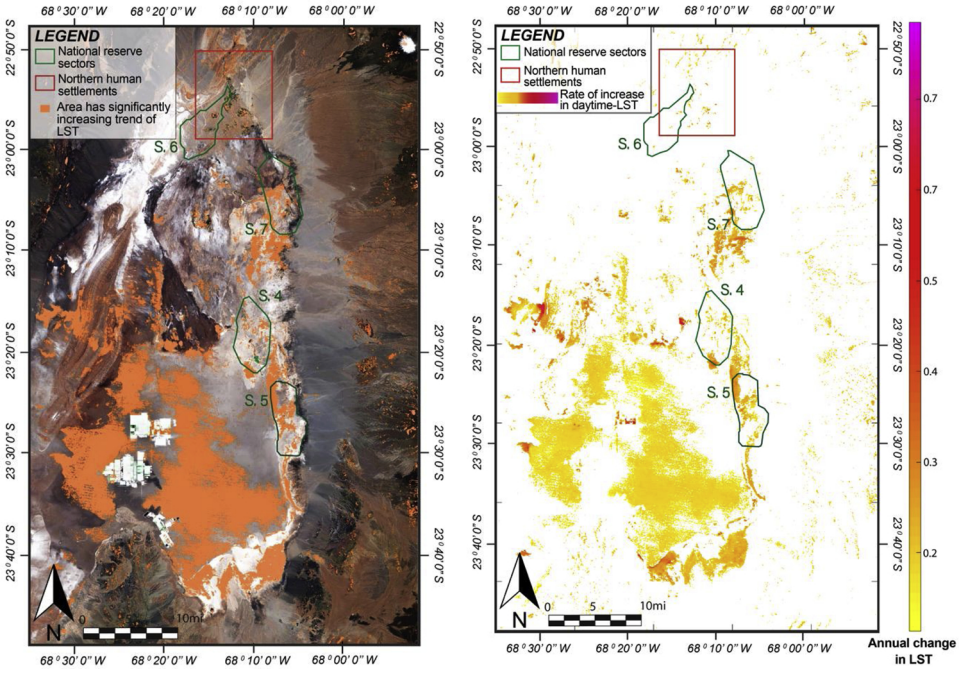

Fig. 8. (a) Map of areas experiencing a significantly increasing trend of daytime Land Surface Temperature (LST) and (b) Map of annual increase rate in LST for LST significantly increased area between 1997 and 2017. Areas surrounding mining operations are having the most severe level of increase in daytime-LST in terms of the impact areas, while the increase is slower than other areas. The national reserved sectors S.4, S.5 and S.7 are also widely impacted by the increasing LST.

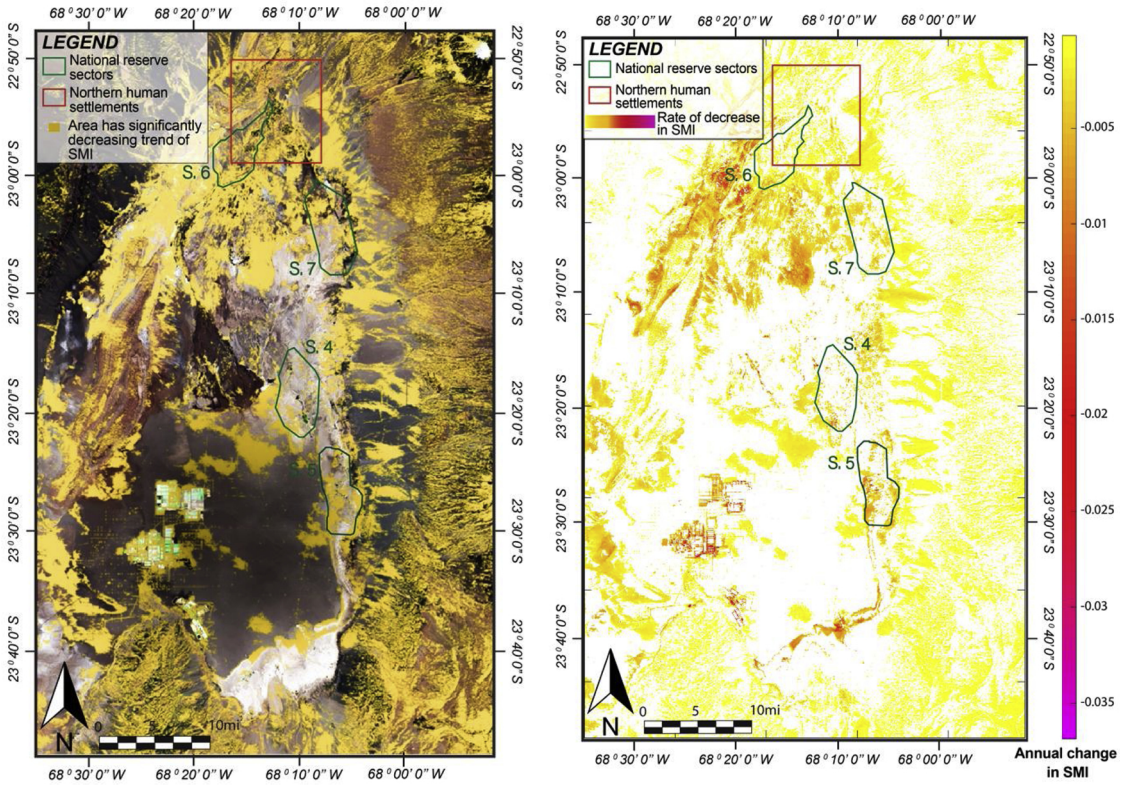

Fig. 9. (a) Map of area experiencing a significantly decreasing trend of soil moisture and (b) Map of annual decrease rate in Soil Moisture Index (SMI) for SMI significantly decreased area between 1997 and 2017. The decreasing trend of soil moisture is prevalent in the study area including national reserve sectors. Edges of lithium ponds and southeastern margins of the ASF show a faster rate of decline compared to the surrounding areas.

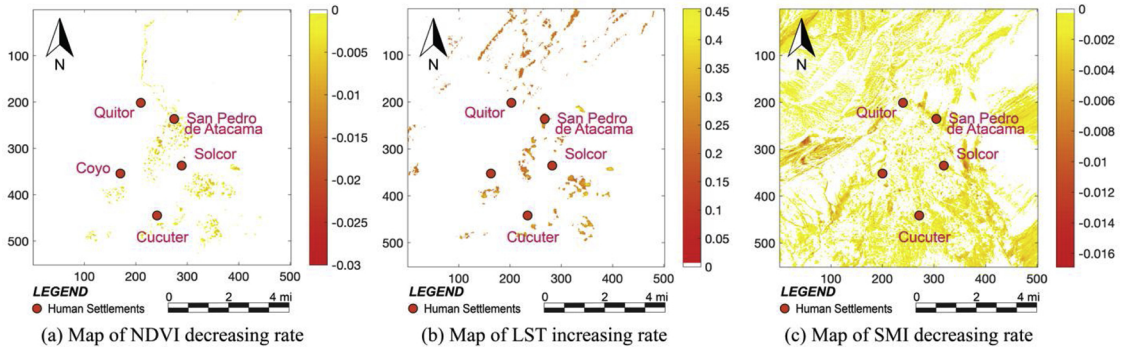

Fig. 10. Annual change of degradation in the northern human settlements on (a) Normalized Difference Vegetation Index (NDVI), (b) Daytime Land Surface Temperature (LST), and (c) Soil Moisture Index (SMI). These areas are experiencing a degrading vegetation cover at a similar rate and a warmer climate at a relatively faster rate. The increasing drought condition is prevalent in most of the areas without a clear spatial pattern.

values of SMI for areas with a significantly decreasing trend of soil moisture also shows a strong negative correlation (p-value = 0.000, R2 = 0.6476). The result implies as mining area increases 1 km2, the SMI value drops down by 0.0007 (Fig. 11b).

The relationship between mining expansion and LST was examined for both summer and winter. The regression of summertime mean LST on mining area has a calculated p-value ≤ 0.05 (p-value = 0.013) while $R^2 \leq 0.5$ (R^2 = 0.3103). We consider mining expansion still have certain explanatory power for the increasing temperature in summer since the relatively small R^2 value can be attributed to the small sample size. Mining area shows a strong correlation with the increasing temperature in wintertime with a calculated p-value ≤ 0.05 and $R^2 > 0.5$ (p-value = 0.001, R^2 = 0.5109). Based on our regression results, as mining operation expands 1 km^2, daytime-LST increases 0.0486 °C in summer and 0.0763 °C in winter correspondingly (Fig. 11c, d).

5. Discussion

5.1. Areas affected by environmental degradation

With respect to the first research question (*which parts in the studied area have been experienced environmental degradation in the past 20 years (1997–2017), in terms of mining land use, vegetation cover, and micro-climate?)*, analyses of environmental indicators examined in this study demonstrate that the ASF and its surrounding areas are experiencing environmental degradation in terms of the degrading vegetation cover, hotter local climate, and increasing dry conditions. Although the overall rate of degradation is relatively slow, the impacted areas are broad, including salt flats, human-settled villages, and national reserved areas. However, this study didn't detect enough changes in nighttime-LST and ET over the past 20 years. This result indicates that the relatively coarse resolution of MODIS may not be appropriate to the

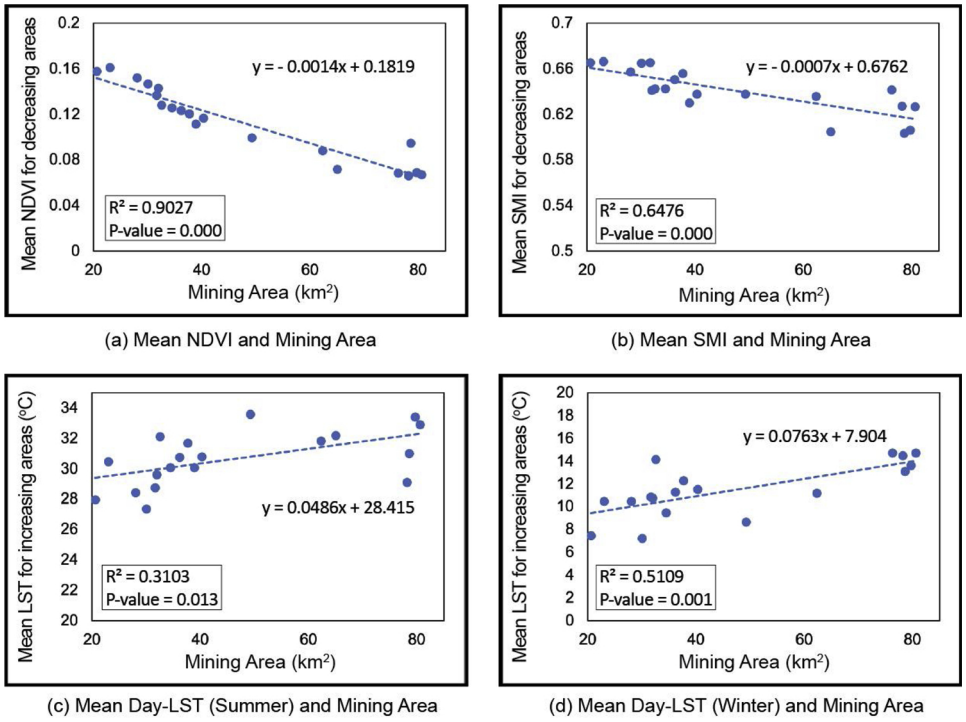

Fig. 11. Correlation of lithium mining expansion and environmental degradation. Mining expansion has a sufficient explanatory power to suggest the degrading vegetation cover, hotter local climate, and the dryer conditions in this study area over the past 20 years.

Table 1
Total area of environmental degradation.

Indicators / Study Area		NDVI		LST		SMI	
		Area (km^2)	Average Rate (NDVI value/yr	Area (km^2)	Average Rate (°C/yr)	Area (km^2)	Average Rate (SMI value/yr
Total study area		59.94	−0.0041	919.31	0.2231	2214.51	−0.0024
Northern human settlements		3.43	−0.0037	5.09	0.2354	72.16	−0.0018
Los Flamencos National Reserve	S.4	0.45	−0.0039	5.03	0.2439	21.69	−0.0035
	S.5	0.18	−0.0028	10.19	0.2309	20.05	−0.0033
	S.6	0.10	−0.0007	0.10	0.1999	25.23	−0.0034
	S.7	0.04	−0.0036	12.42	0.2588	26.00	−0.0030

environment of ASF where both natural and man-made features are sparsely distributed. In general, the increasing drought condition is prevalent in our study area, where 26.7% of the total area is having increasingly drier soil (Table 1).

Areas located in mining operations are experiencing a comparatively faster rate of environmental degradation, especially for turning salt flats to operation ponds and increasing drought conditions. Although the temperature rise is relatively slow in these areas, areas close to operation sites are still experiencing a hotter climate in a faster than average rate. In general, large areas within the ASF are impacted by the hotter climate and the land transformation to mining ponds.

Human settlement areas in the north are experiencing environmental degradation at a rate similar to the average level (Table 1). Over the past 20 years, 3.43 km^2 of vegetated lands in the northern human-settled region have been undergoing degradation, including the disappearance of tree covers and changing to sparse and lower density vegetation. The degradation trend of vegetation oases in human clustered areas may confirm the results from an empirical study (Babidge and Bolados, 2018) stating that many locals abandoned their agriculture land due to the lack of water. Besides, 5.09 km^2 of these areas are going through hotter and hotter climate, and 72.16 km^2 are changing to much drier conditions (Table 1).

Four national reserve sectors in our study area are affected by the increasing drought condition, while S.5 and S.7 are even more impacted by the hotter climate. A total of 92.97 km^2 of national reserved lands are experiencing a significantly increasing drought condition in soil; and 27.74 km^2 are becoming warmer during the daytime over the past 20 years (Table 1). However, areas with the decreasing value of NDVI in the sector S.4 and S.5 cannot be simply considered as the degrading vegetation cover since these sectors are composed of wetlands and lagoons. There is still about 0.14 km^2 of vegetated lands in the S.6 and S.7 are degraded.

Climatic variabilities in the study period may also affect the examined environmental conditions in the study area, even after we have reduced certain variabilities from local weather changes in the process of data selection and statistical trend test. In the desert environment, rare precipitation events may contribute considerably less than the impact-intensive anthropogenic stressors on the local environment. Marazuela et al. (2019b) observed the decrease of evaporation rate after mining operations in the ASF, indicating a decline of the water table and depletion of soil moisture due to mining activities. The short-term changes in local weather may also have limited influence on vegetation health in the hyper-arid environment. Díaz et al. (2019) found that annual and perennial plants are extraordinarily resilient in response to climate variability in interannual (years to decades) time frame. Moreover, herbaceous plants that are relatively vulnerable to

Table 2
Weighting sets of four scenarios.

Scenarios	Standardized NDVI change	Standardized LST change	Standardized SMI change
Scenario 1	0.33	0.33	0.33
Scenario 2	0.5	0.25	0.25
Scenario 3	0.25	0.5	0.25
Scenario 4	0.25	0.25	0.5

short-term variabilities, have a low presence in the Atacama Desert. However, existing research is still inadequate to provide a sound reference to the local climate variability in temperature and precipitation. Thus, the impact from climate variability on environmental degradations identified in this study still need future scrutiny.

5.2. Environmental degradation index

To provide the overall environmental health of the study area, we introduced a Degradation Index (DI) using a weighted combination of changes in environmental indicators examined in this study. We firstly retained all pixels showing negative environment changes and standardized the change rate of each indicator to the range from 0 towards 1, which corresponds to changes from relatively slow to fast. The standardized indicators were then weighted and summed to generate DI with a valid range from 0 to 1. The resulted DI values were classified into 6 classes: no degradation (DI = 0), barely degraded (0–0.2), less degraded (0.2 − 0.4), moderately degraded (0.4 − 0.6), highly degraded (0.6 − 0.8), severely degraded (0.8–1). We considered four scenarios with different weighting sets, one with equal weights to indicators and the rest scenarios with one indicator assigned a higher weight (Table 2). For each pixel, the scenario that produced the lowest DI was selected as the best scenario, and the difference between the lowest DI and mean DI of four scenarios was defined as uncertainty. The area with high uncertainty indicates the degradation degree could be worse than in the best-case scenario. Subsequently, we generated: (1)a map of the best-scenario DI and (2) a map of DI uncertainty showing the spatial distribution of the lowest possible environmental degradation and its uncertainty. The resulted map for each scenario is provided in the Supplementary Information (SI-Fig. 1).

The best-case scenario (Fig. 12a) and scenario uncertainty (Fig. 12a) map reveal some insights on the level and uncertainty of degradation. Most areas in the study region are barely or less degraded with relatively low uncertainty. However, some human settlement areas (highlighted in red box) in the northern part of the region show a moderate to high level of degradation with relatively high uncertainty. Mining areas within the ASF are moderately degraded with high uncertainty. Most national reserve areas (S.4-S.7) are having less or bare degradation, while a few areas still indicate moderate to high level of degradation. Other areas showing a moderate or high degradation level are also having relatively high uncertainty level.

In general, most of the areas are barely or less degraded with low uncertainties, whereas areas moderately to highly degraded are also associated with higher uncertainty, implying that these areas may encounter a worse level of degradation. Therefore, we suggest that the moderately to highly degraded areas may need more attentions from local decision-makers and environmental inspectors, especially for areas with human settlements and national reserved lands.

5.3. Anthropogenic stressors on the local environment

With respect to the second research question (*What is the relationship between the expanding lithium industry and dynamic patterns of environmental degradation in this area?)*, it is found that the fast expansion of lithium mining operations in the ASF is found to have a strong correlation with the ongoing environmental degradation in the study area. The expanding lithium industry may be one of the important environmental stressors to the overall health of the local environment, especially for the factors we examined.

To complicate the issue of mining environmental impacts, the lithium mining companies in the ASF have been accusing each other of extracting more brine than what is permitted since 2013. The impact caused by lithium extraction is hard to track because mining companies made changes on how they monitor wells without authorization, according to a Chile's environmental regulator (Reuters, 2018). The environmental degradation identified in this study accords with results from a study on the availability of water in the ASF by CORFO (CORFO, 2018), that more water and brine was leaving the system through pumping and evaporation than was coming back in through precipitations. These results are also consistent with findings from government inspection reports (SMA, 2016) that about 32.4% of the native Algarrobo trees on SQM's (a mining company) property were dying since 2013. The disappearance of the native Algarrobo trees, which are drought-tolerant species by sending roots deep into the underground to survive, implies a water shortage in the ASF aquifer and may act as an early warning signal of water scarcity problems.

However, potential environmental stressors other than the mining industry, such as the booming tourism and population increase, may also have negative impacts on the health of the local environment. The explosion of tourism in the region of ASF since the 1990s has dramatically increased the local population as well as the flows of tourists (RIDES (Research and Resources for Sustainable Development), 2005). During high seasons, the population of tourists could reach more than double the local population (RIDES (Research and Resources for Sustainable Development), 2005). Over the past 15 years, the number of tourists attracted to the Los Flamencos National Reserve has increased twelve-fold, reaching 0.4 million tourists in 2016 (INE (National Statistics Institute of Chile), 2003, 2017). The booming tourism industry can increase both direct and indirect water use, therefore adding water stress to already water scares destinations (Gössling et al., 2012). Based on an estimated daily water consumption of 200 L/tourist in Chile (Gössling, 2006), at least about 83,736,800 L of water was consumed in 2016 in the ASF if each tourist only spends one day there. The increasing tourist flows could pose more stress on the local drought condition and warmer climate through water consumption, but may also present other ecological impacts on the local ecosystem such as vegetation degradation and waste production.

The notable population growth driven by the booming lithium industry and tourism opportunities could also have contributed to the environmental degradation identified in this study in both direct and indirect ways. Currently, according to the national census in 2017 (INE (National Statistics Institute of Chile), 2018a), the local population has doubled over the past 15 years and reach 10,996 in 2017, overshooting the projected population by almost 40% (INE (National Statistics Institute of Chile), 2018b). Therefore, the resulting increased water consumption and other human activities could attribute to the warmer and drier local climate. On the other hand, the availability of wage labor provided by the lithium mining industry has attracted great labor forces and significantly driven most villagers to shift from the agriculture and pastoralism lifestyle to a neoliberal cash economy (Babidge, 2013). Nowadays, more and more villagers have worked as wage labors or contractors for lithium companies, leaving agriculture as only supplementary to a cash economy (Babidge, 2013). Hence, the less attention on pastoral and agricultural sites could partly explain the vegetation degradation.

6. Conclusions

The continuously expanding mining industry is investigated to be one of the critical environmental stressors to the overall health of the local environment. Other possible stressors, such as the explosive tourism industry and population increase, are still lacking investigation,

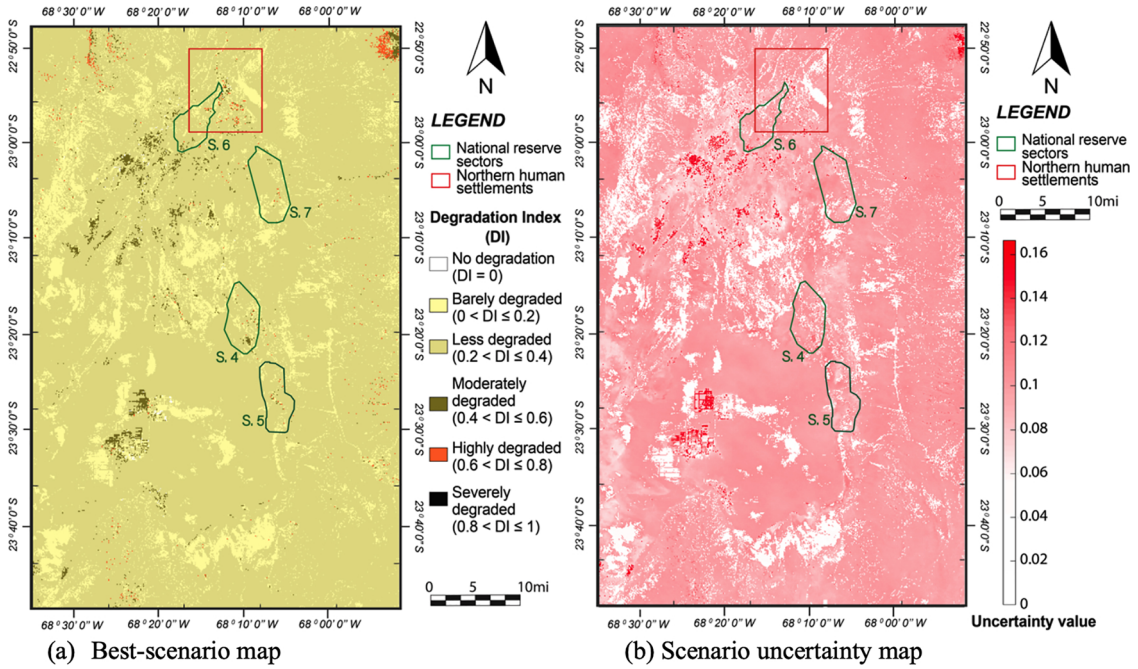

Fig. 12. (a) Spatial map showing the best-case scenario of environmental degradation based on the four different scenarios examined in the study area; (b) Spatial map showing the uncertainty in the best-scenario map; the deeper color in red indicates a higher level of uncertainty compared to other scenarios.

which may require future research to detect their effects on the local environment. In their efforts to manage future lithium mining expansion, policy makers need to pay more attention to areas that have been experiencing increasing LST, decreasing NDVI, and increasing drought conditions in soil, especially in national reserved lands. We anticipate that our analysis of lithium mining and environmental degradation will help mining regulators, local environmental regulators, lithium industry decision-makers, and national park managers provide better management of the world's largest lithium production sites for a sustainable future and that our analysis will assist in future research to reveal other stressors to the local environmental degradation and possible impacts along the lithium-based transportation pathway.

Acknowledgment

The authors thank the anonymous reviewers for their comments that helped improving the manuscript.

Appendix A. Supplementary data

Supplementary data associated with this article can be found, in the online version, at https://doi.org/10.1016/j.jag.2019.04.016

References

Agusdinata, D., Liu, W., Eakin, H., Romero, H., 2018. Socio-environmental impacts of lithium mineral extraction: towards a research agenda. Environ. Res. Lett. 13 (12), 123001.
USGS Mineral Commodity Summaries. https://minerals.usgs.gov/minerals/pubs/commodity/lithium/.
Artis, D.A., Carnahan, W.H., 1982. Survey of emissivity variability in thermography of urban areas. Remote Sens. Environ. 12 (4), 313–329.
Avdan, U., Jovanovska, G., 2016. Algorithm for automated mapping of land surface temperature using LANDSAT 8 satellite data. J. Sens. 2016, 1–8.
Babidge, S., 2013. "Socios": the contested morality of "partnerships" in indigenous community-mining company relations, Northern Chile. J. Lat. Am. Caribb. Anthropol. 18 (2), 274–293.
Babidge, S., 2016. Contested value and an ethics of resources: water, mining and indigenous people in the Atacama desert, Chile. Aus. J. Anthrop. 27 (1), 84–103.
Babidge, S., Bolados, P., 2018. Neoextractivism and Indigenous Water Ritual in Salar de Atacama, Chile. Lat. Am. Perspect. 45 (5), 170–185.
Carter, G., 1998. Reflectance wavebands and indices for remote estimation of photosynthesis and stomatal conductance in pine canopies. Remote Sens. Environ. 63 (1), 61–72.
Chen, X., Zhao, H., Li, P., Yin, Z., 2006. Remote sensing image-based analysis of the relationship between urban heat island and land use/cover changes. Remote Sens. Environ. 104 (2), 133–146.
CORFO (Production Development Corporation of Chile), 2018. Fiscal Instructor de la División de Sanción y Cumplimiento Superintendencia del Medio Ambiente (in Spanish). Retrieved from. CORFO, Santiago, Chile. https://www.documentcloud.org/documents/5003677-Presentaci%C3%B3N-CORFO.html#document/p3/a461155.
Deetman, S., Pauliuk, S., van Vuuren, D., van der Voet, E., Tukker, A., 2018. Scenarios for demand growth of metals in electricity generation technologies, cars, and electronic appliances. Environ. Sci. Technol. 52 (8), 4950–4959.
DeFries, R., Townshend, J., 1994. NDVI-derived land cover classifications at a global scale. Int. J. Remote Sens. 15 (17), 3567–3586.
Díaz, F.P., et al., 2019. Multiscale climate change impacts on plant diversity in the Atacama desert. Glob. Change Biol. 2019, 1–13.
Estoque, R., Myint, S., Wang, C., Ishtiaque, A., Aung, T., Emerton, L., Ooba, M., Hijioka, Y., Mon, M., Wang, Z., Fan, C., 2018. Assessing environmental impacts and change in Myanmar's mangrove ecosystem service value due to deforestation (2000–2014). Glob. Change Biol. 24 (11), 5391–5410.
Fan, C., Myint, S., Rey, S., Li, W., 2017. Time series evaluation of landscape dynamics using annual Landsat imagery and spatial statistical modeling: evidence from the Phoenix metropolitan region. Int. J. Appl. Earth Obs. Geoinf. 58, 12–25.
Flexer, V., Baspineiro, C.F., Galli, C.I., 2018. Lithium recovery from brines: a vital raw material for green energies with a potential environmental impact in its mining and processing. Sci. Total Environ. 639, 1188–1204.
Gössling, S., Peeters, P., Hall, C., Ceron, J., Dubois, G., Lehmann, L., Scott, D., 2012. Tourism and water use: supply, demand, and security. An international review. Tour. Manage. 33 (1), 1–15.
Gössling, S., 2006. Tourism and water. In: Gössling, S., Hall, C.M. (Eds.), Tourism & Global Environmental Change: Ecological, Social, Economic and Political Interrelationships. Routledge, Abingdon, UK, pp. 180–194.
Habashi, F., 1997. Handbook of Extractive Metallurgy. Wiley-VCH.
Hansen, M., DeFries, R., Townshend, J.R., Sohlberg, R., 2000. Global land cover classification at 1 km spatial resolution using a classification tree approach. Int. J. Remote Sens. 21 (6–7), 1331–1364.
IFC (International Finance Corporation), 2017. Energy Storage Trends and Opportunities in Emerging Markets. IFC, Boulder USA.
INE (National Statistics Institute of Chile), 2003. Turismo Informe Annual 2002. INE, Santiago, Chile.
INE (National Statistics Institute of Chile), 2017. Turismo Informe Annual 2016. INE, Santiago, Chile.
INE (National Statistics Institute of Chile), 2018a. National Population and Housing Census Redatam-2017. Retrieved from. http://www.ine.cl/estadisticas/demograficas-y-vitales.
INE (National Statistics Institute of Chile), 2018b. Estimaciones y Proyecciones de La Población de Chile 1992-2050 Total País. Retrieved from. http://www.ine.cl/estadisticas/demograficas-y-vitales.
Ishtiaque, A., Myint, S., Wang, C., 2016. Examining the ecosystem health and

sustainability of the world's largest mangrove forest using multi-temporal MODIS products. Sci. Total Environ. 569–570, 1241–1254.
Jaskula, B.W., 2017. Lithium: Mineral Commodity Summaries (2017). United States Geological Survey, Reston, VA.
Jaskula, B.W., 2018. Lithium: Mineral Commodity Summaries (2018). United States Geological Survey, Reston, VA.
Joyce, A.O., 1998. Lithium: Mineral Commodity Summaries (1998). United States Geological Survey, Reston, VA.
Kampf, S., Tyler, S., Ortiz, C., Muñoz, J., Adkins, P., 2005. Evaporation and land surface energy budget at the Salar de Atacama, Northern Chile. J. Hydrol. 310 (1-4), 236–252.
Kendall, M.G., 1948. Rank Correlation Methods, 4th ed. 1970. Charles Griffin and Co., Ltd., London, UK.
Lee, R., Yu, F., Price, K., Ellis, J., Shi, P., 2002. Evaluating vegetation phenological patterns in Inner Mongolia using NDVI time-series analysis. Int. J. Remote Sens. 23 (12), 2505–2512.
Li, Z., Tang, B., Wu, H., Ren, H., Yan, G., Wan, Z., Trigo, F., Sobrino, I.A., 2013. Satellite-derived land surface temperature: current status and perspectives. Remote Sens. Environ. 131, 14–37.
Mann, H.B., 1945. Nonparametric tests against trend. Econometrica 13, 245–259.
Marazuela, M.A., Vázquez-Suñé, E., Ayora, C., García-Gil, A., Palma, T., 2019a. Hydrodynamics of salt flat basins: the Salar de Atacama example. Sci. Total Environ. 651, 668–683.
Marazuela, M.A., Vázquez-Suñé, E., Ayora, C., García-Gil, A., Palma, T., 2019b. The effect of brine pumping on the natural hydrodynamics of the Salar de Atacama: the damping capacity of salt flats. Sci. Total Environ. 654, 1118–1131.
Molina Camacho, F., 2016. Intergenerational dynamics and local development: mining and the indigenous community in Chiu Chiu, El Loa Province, northern Chile. Geoforum 75, 115–124.
Mu, Q., Heinsch, F.A., Zhao, M., Running, S.W., 2007. Development of a global evapotranspiration algorithm based on MODIS and global meteorology data. Remote Sens. Environ. 11, 519–536.
Myneni, R., Hall, F., Sellers, P., Marshak, A., 1995. The interpretation of spectral vegetation indexes. IEEE Trans. Geosci. Remote 33 (2), 481–486.
Ngie, A., Abutaleb, K., Ahmed, F., Darwish, A., Ahmed, M., 2014. Assessment of urban heat island using satellite remotely sensed imagery: a review. S. Afr. Geogr. J. 96 (2), 198–214.
Nishishiba, M., Jones, M., Kraner, M., 2014. Bivariate correlation. Research Methods and Statistics for Public and Nonprofit Administrators: A Practical Guide. Sage Publications, US, pp. 223–238.
Pettorelli, N., Vik, J., Mysterud, A., Gaillard, J., Tucker, C., Stenseth, N., 2005. Using the satellite-derived NDVI to assess ecological responses to environmental change. Trends Ecol. Evol. 20 (9), 503–510.
Reed, B.C., Brown, J.F., VanderZee, D., Loveland, T.R., Merchant, J.W., Ohlen, D.O., 1994. Measuring phenological variability from satellite imagery. J. Veg. Sci. 5 (5), 703–714.
Reuters, 2018. A Water Fight in Chile's Atacama raises Questions over Lithium Mining. published on October 18. Retrieved from. https://www.reuters.com/article/us-chile-lithium-insight/a-water-fight-in-chiles-atacama-raises-questions-over-lithium-mining-idUSKCN1MS1L8.
RIDES (Research and Resources for Sustainable Development), 2005. Millennium Ecosystem Assessment: Human well-being and sustainable management in San Pedro de Atacama, Chile – Executive report. RIDES, Santiago, Chile.
Romero, H., Méndez, M., Smith, P., 2012. Mining development and environmental injustice in the Atacama Desert of Northern Chile. Environ. Justice 5 (2), 70–76.
Running, S.W., 1990. Estimating primary productivity by combining remote sensing with ecosystem simulation. In: Hobbs, R.J., Mooney, H.A. (Eds.), Remote Sensing of Biosphere Functioning. Springer-Verlag Inc., New York, USA, pp. 65–86.
Salas, J., Guimerà, J., Cornellà, O., Aravena, R., Guzmán, E., Tore, C., von Igel, W., Moren, R., 2010. Hidrogeología del sistema lagunar del margen este del Salar de Atacama (Chile). Boletín Geológico y Minero 121 (4), 357–372.
Schiebe, F.R., Harrington Jr, J.A., Ritchie, J.C., 1992. Remote sensing of suspended sediments: the Lake Chicot, Arkansas project. Int. J. Remote Sens. 13 (8), 1487–1509.
Sen, P.K., 1968. Estimates of the regression coefficient based on Kendall's tau. J. Am. Stat. Assoc. 63, 1379–1389.
Seto, K.C., Fragkias, M., Güneralp, B., Reilly, M.K., 2011. A meta-analysis of global urban land expansion. PLoS One 6 (8), e23777.
SMA (Superintendency of the Environment of Chile), 2016. Formula Cargos Que Indica a SQM Salar S.A. Retrieved from. SMA, Santiago, Chile. https://www.documentcloud.org/documents/5003676-Formulaci%C3%B3N-De-Cargos.html#document/p14/a461122?.
Stamp, A., Lang, D., Wäger, P., 2012. Environmental impacts of a transition toward e-mobility: the present and future role of lithium carbonate production. J. Clean. Prod. 23 (1), 104–112.
Steel, R.G., Torrie, J.H., 1980. Principles and Procedures of Statistics: a Biometrical Approach, second ed. McGraw-Hill, New York.
Studer, S., Stöckli, R., Appenzeller, C., Vidale, P.L., 2007. A comparative study of satellite and ground-based phenology. Int. J. Biometeorol. 51 (5), 405–414.
Tran, T., Luong, V.T., 2015. Lithium production processes. In: In: Chagnes, A., Świątowska, J. (Eds.), Lithium Process Chemistry 2015. Elsevier, pp. 81–124.
Wang, C., Myint, S., Wang, Z., Song, J., 2016. Spatio-temporal modeling of the urban heat island in the phoenix metropolitan area: land use change implications. Remote Sens. 8 (3), 185.
Wang, C., Wang, C., Myint, S., Wang, Z., 2017. Landscape determinants of spatio-temporal patterns of aerosol optical depth in the two most polluted metropolitans in the United States. Sci. Total Environ. 609, 1556–1565.
Yang, J., Gong, P., Fu, R., Zhang, M., Chen, J., Liang, S., Xu, B., Shi, J., Dickinson, R., 2013. The role of satellite remote sensing in climate change studies. Nat. Clim. Change 3 (1), 875–883.
Zhan, Z., Qin, Q., Abduwasit, G., Wang, D., 2007. NIR-red spectral space based new method for soil moisture monitoring. Sci. China Ser. D Earth Sci. 50 (2), 283–289.